

See discussions, stats, and author profiles for this publication at: <https://www.researchgate.net/publication/235376560>

# Structural, kinetic and computational investigation of *Vitis vinifera* DHDPS reveals new insight into the mechanism of lysine-mediated allosteric inhibition

ARTICLE *in* PLANT MOLECULAR BIOLOGY · JANUARY 2013

Impact Factor: 4.26 · DOI: 10.1007/s11103-013-0014-7 · Source: PubMed

CITATIONS

5

READS

67

8 AUTHORS, INCLUDING:



[Renwick C J Dobson](#)

University of Canterbury

83 PUBLICATIONS 1,173 CITATIONS

[SEE PROFILE](#)



[Juliet A Gerrard](#)

University of Auckland

152 PUBLICATIONS 2,712 CITATIONS

[SEE PROFILE](#)



[John Wagner](#)

IBM Research

45 PUBLICATIONS 3,915 CITATIONS

[SEE PROFILE](#)



[Matthew A Perugini](#)

La Trobe University

109 PUBLICATIONS 2,571 CITATIONS

[SEE PROFILE](#)

# Structural, kinetic and computational investigation of *Vitis vinifera* DHDPS reveals new insight into the mechanism of lysine-mediated allosteric inhibition

Sarah C. Atkinson · Con Dogovski · Matthew T. Downton · Peter E. Czabotar ·  
Renwick C. J. Dobson · Juliet A. Gerrard · John Wagner · Matthew A. Perugini

Received: 12 November 2012 / Accepted: 15 January 2013 / Published online: 26 January 2013  
© Springer Science+Business Media Dordrecht 2013

**Abstract** Lysine is one of the most limiting amino acids in plants and its biosynthesis is carefully regulated through inhibition of the first committed step in the pathway catalyzed by dihydrodipicolinate synthase (DHDPS). This is mediated via a feedback mechanism involving the binding of lysine to the allosteric cleft of DHDPS. However, the precise allosteric mechanism is yet to be defined. We present a thorough enzyme kinetic and thermodynamic analysis of lysine inhibition of DHDPS from the common grapevine, *Vitis vinifera* (Vv). Our studies demonstrate that lysine binding is both tight (relative to bacterial DHDPS orthologs) and cooperative. The crystal structure of the enzyme bound to lysine (2.4 Å) identifies the allosteric binding site and clearly shows a conformational change of several residues within the allosteric and active sites. Molecular dynamics simulations comparing the lysine-bound (PDB ID 4HNN) and lysine free (PDB ID 3TUU) structures show that Tyr132, a key catalytic site residue,

undergoes significant rotational motion upon lysine binding. This suggests proton relay through the catalytic triad is attenuated in the presence of lysine. Our study reveals for the first time the structural mechanism for allosteric inhibition of DHDPS from the common grapevine.

**Keywords** Allostery · Analytical ultracentrifugation · Circular dichroism spectroscopy · Dihydrodipicolinate synthase · Enzyme · Grapevine · Lysine biosynthesis · Molecular dynamics simulations · X-ray crystallography

ASA	(S)-Aspartate semialdehyde
DHDPR	Dihydrodipicolinate reductase
DHDPS	Dihydrodipicolinate synthase
Pyr	Pyruvate
Lysine	(S)-Lysine
Threonine	(S)-Threonine
Vv	<i>Vitis vinifera</i>

**Electronic supplementary material** The online version of this article (doi:10.1007/s11103-013-0014-7) contains supplementary material, which is available to authorized users.

S. C. Atkinson · C. Dogovski · M. A. Perugini (✉)  
Department of Biochemistry, La Trobe Institute for Molecular  
Science, La Trobe University, Melbourne, VIC 3086, Australia  
e-mail: M.Perugini@latrobe.edu.au

S. C. Atkinson · R. C. J. Dobson · M. A. Perugini  
Department of Biochemistry and Molecular Biology, Bio21  
Molecular Science and Biotechnology Institute, The University  
of Melbourne, 30 Flemington Road, Melbourne, VIC 3010,  
Australia

M. T. Downton · J. Wagner  
IBM Research Collaboratory for Life Sciences-Melbourne,  
Victorian Life Sciences Computation Initiative, Carlton, VIC  
3010, Australia

P. E. Czabotar  
The Walter and Eliza Hall Institute of Medical Research,  
Parkville, VIC 3052, Australia

R. C. J. Dobson · J. A. Gerrard  
Biomolecular Interaction Centre and School of Biological  
Sciences, University of Canterbury, Private Bag 4800,  
Christchurch, New Zealand

J. A. Gerrard  
Industrial Research Limited, PO Box 31310, Lower Hutt  
5040, New Zealand

## Introduction

The grapevine (genus *Vitis*) is one of the world's most economically-important crops that in 2010 generated approximately \$40 billion towards the global economy (Nicholson et al. 2012). A significant proportion of the economic value of grapevine arises from wine production and sales with 4.4 billion litres of wine produced globally in 2010 (Nicholson et al. 2012). Cultivars of the European wine grape (*Vitis vinifera*) form the basis of the majority of wines produced around the world, making it the most cultivated and economically important grape species (Vivier and Pretorius 2002). However, one of the most limiting nutrients in grape is the amino acid, lysine (Igartuburu et al. 1991; Nunan et al. 1997). Indeed, many crops contain low levels of lysine and therefore attempts have been made to increase the lysine content of agriculturally-important plants by classical breeding, mutant selection, or by genetic modification (van der Meer et al. 2001).

Of the enzymes that function in the lysine biosynthesis pathway, dihydrodipicolinate synthase (DHDPS) (Fig. 1) has attracted the most interest in lysine up-regulation (Zhu and Galili 2003). The enzyme is also a promising target for antimicrobial discovery (Cox et al. 2000; Perugini et al. 2005; Hutton et al. 2007; Boughton et al. 2008; Mitsakos et al. 2008; Dogovski et al. 2009; Dogovski et al. 2012). DHDPS catalyses the condensation of pyruvate and (*S*)-aspartate semialdehyde (ASA) to form (4*S*)-4-hydroxy-2,3,4,5-tetrahydro-(2*S*)-dipicolinic acid (HTPA) (Blickling et al. 1997b). The DHDPS catalyzed reaction is the first committed step of the lysine biosynthesis pathway (Fig. 2) (Hutton et al. 2007; Dogovski et al. 2009, 2012; Atkinson et al. 2012). The reaction proceeds via a ping-pong kinetic mechanism in which pyruvate binds and forms a Schiff base to an active-site lysine residue (Lys184 in *V. vinifera*

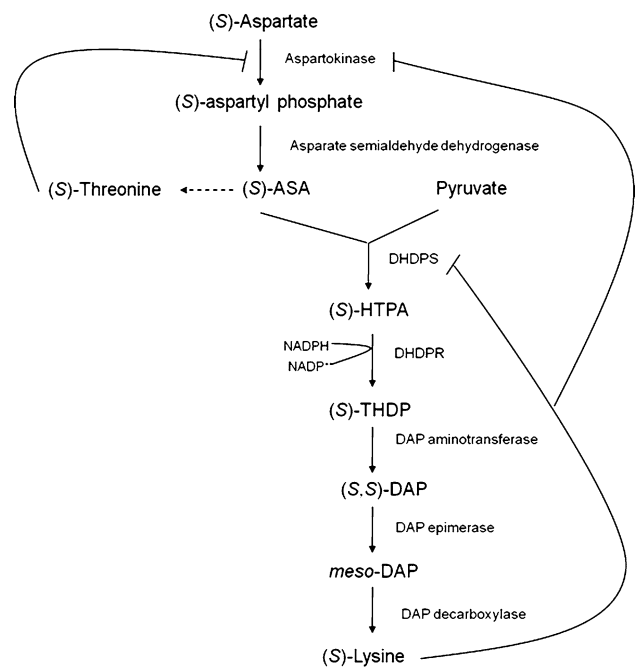
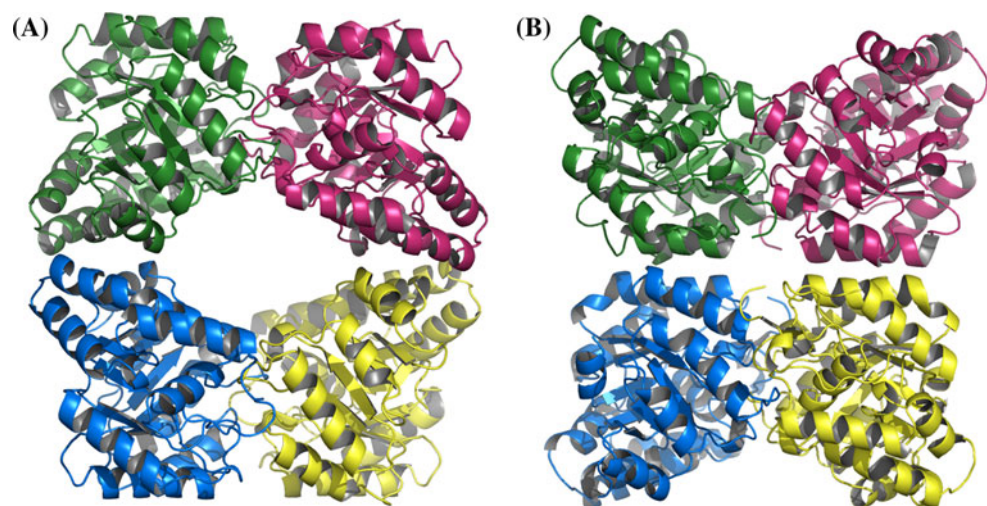


**Fig. 2** Lysine biosynthesis in plants. The biosynthesis of lysine and threonine begins with the phosphorylation of (*S*)-aspartate by aspartokinase to form ASA. The pathways diverge at this point with the first committed step in lysine biosynthesis, namely, the DHDPS catalyzed condensation of pyruvate and ASA to form HTPA. The enzyme DHDPS is allosterically inhibited by lysine whilst aspartokinase is allosterically inhibited by lysine and threonine

DHDPS). ASA then reacts with the resultant enamine and following cyclization forms the product HTPA (Blickling et al. 1997b). HTPA is then converted in several enzymatic steps to lysine (Fig. 2) (Hutton et al. 2007; Dogovski et al. 2009, 2012).

The structure of DHDPS has been studied extensively in a number of bacteria (Mirwaldt et al. 1995; Dobson et al. 2005b; Blagova et al. 2006; Burgess et al. 2008; Devenish

**Fig. 1** Structure of DHDPS from bacteria and plants. Dihydrodipicolinate synthase from **a** *E. coli* (PDB ID: 2XYC) and **b** *V. vinifera* (PDB:3TUU). Figure adapted from (Atkinson et al. 2012)



et al. 2008; Dobson et al. 2008; Girish et al. 2008; Kefala et al. 2008; Voss et al. 2010). The bacterial form of the enzyme usually consists of a homotetramer of four identical ( $\beta/\alpha$ )<sub>8</sub>-barrel monomers (Fig. 1a), with the active site situated near the center of the barrel. The tetramer can be described as a dimer of tight dimers, with two tight-dimers binding in a ‘head-to-head’ manner (Dobson et al. 2005b; Voss et al. 2010). By contrast, DHDPS enzymes from plants have been less extensively studied. The enzyme is encoded by the nuclear localized *dapA* gene and imported into plastids where DHDPS functions (Ghislain et al. 1990; Shaul and Galili 1992a; Vauterin and Jacobs 1994). We recently determined the crystal structure of DHDPS from *V. vinifera* (Atkinson et al. 2012), which, along with that of DHDPS from *Arabidopsis thaliana* (Griffin et al. 2012) and *Nicotiana sylvestris* (Blickling et al. 1997a) also forms a homotetramer, or dimer of tight dimers, but with an alternative architecture to that observed in bacteria referred to as a ‘back-to-back’ dimer-of-dimers (Fig. 1b).

The lysine biosynthetic pathway in plants is regulated by several feedback inhibition loops (Fig. 2). Aspartokinase, the first enzyme in the pathway, is feedback inhibited by lysine and threonine; whilst DHDPS is feedback inhibited by the final product of the pathway, lysine. Evidence suggests that DHDPS is the main regulatory point in higher plants, given that *N. sylvestris* mutants with lysine-desensitized DHDPS overproduce lysine (Frankard et al. 1992), whereas mutants that have aspartokinase desensitized to lysine inhibition overproduce threonine (Shaul and Galili 1992b).

The negative feedback inhibition of DHDPS by lysine has been investigated in several Gram-negative bacteria, Gram-positive bacteria, and also plant species. DHDPS from Gram-negative bacteria such as *Escherichia coli* (Yugari and Gilvarg 1965; Soares da Costa et al. 2010) and *Neisseria meningitidis* (Devenish et al. 2009) are weakly inhibited with  $IC_{50}$  values ranging from 0.25 to 1.0 mM. Whereas, DHDPS from Gram-positive bacteria such as *Bacillus licheniformis* (Halling and Stahly 1976), *Bacillus megaterium* (Webster and Lechowich 1970), *Bacillus subtilis* (Yamakura et al. 1974), *Bacillus anthracis* (Blagova et al. 2006; Domigan et al. 2009; Voss et al. 2010), *Corynebacterium glutamicum* (Cremer et al. 1988), *Bacillus cereus* (Hoganson and Stahly 1975), *Lactobacillus plantarum* (Cahyanto et al. 2006) and methicillin-resistant *Staphylococcus aureus* (MRSA) (Burgess et al. 2008) show no inhibition by lysine, including concentrations higher than is considered physiologically relevant (up to 50 mM). By contrast, DHDPS from the plant species *Triticum aestivum* (Kumpaisal et al. 1987), *Daucus carota sativa* (Matthews and Widholm 1979), *Spinacia oleracea* (Wallsgrave and Mazelis 1980), *Zea mays* (Frisch et al.

1991) and *Pisum sativum* (Dereppe et al. 1992) are strongly inhibited by lysine with  $IC_{50} = 10\text{--}50\text{ }\mu\text{M}$ . It is therefore not surprising that lysine is one of the most limiting amino acids in plants.

Accordingly, a range of transgenic plants have been developed in which DHDPS has been genetically manipulated with the aim of producing high-lysine crops (Frankard et al. 1992; Perl et al. 1992; Shaul and Galili 1992a; Galili 1995; Ghislain et al. 1995; Kwon et al. 1995; Bittel et al. 1996; Brinch-Pedersen et al. 1996; Silk and Matthews 1997). The introduction of feedback-insensitive DHDPS enzymes that lack the propensity to bind lysine allosterically resulted in a 10 to 100-fold overproduction of lysine (Negrutiu et al. 1984; Frankard et al. 1992; Shaul and Galili 1993; Ben-Tzvi Tzchori et al. 1996; Sarrobert et al. 2000). This demonstrates that removal of lysine-mediated allosteric inhibition greatly influences the lysine content of plants.

Kinetic and structural studies show that lysine is an allosteric inhibitor causing partial inhibition (90 %) at saturating concentrations (Yugari and Gilvarg 1965). The structure of *E. coli* DHDPS co-crystallized with lysine (PDB ID: 1YXD) revealed two lysine molecules bind the allosteric site in a back-to-back orientation with the alpha carbon of each lysine separated by 4.10 Å (Dobson et al. 2005b). Isothermal titration microcalorimetry (ITC) experiments show that inhibition is cooperative with the second molecule of lysine binding  $10^5$  times more tightly than the first (Phenix and Palmer 2008; Muscroft-Taylor et al. 2010). In addition, a structural study of DHDPS from the plant *N. sylvestris* suggests a conformational change occurs upon lysine binding (Blickling et al. 1997a). Several of the residues involved in contacts at the tight dimer interface are displaced when lysine is bound, dislocating the dimers in relation to each other. However, this altered conformation was not observed in the *E. coli* DHDPS structure bound to lysine (Dobson et al. 2005). Therefore, the precise mechanism of lysine-mediated allosteric inhibition of DHDPS remains elusive.

Here, we present thorough kinetic and thermodynamic analyses of lysine-mediated allosteric inhibition in DHDPS from *V. vinifera* (Vv-DHDPS). We also describe the crystal structure of the enzyme bound to lysine (2.4 Å); and subsequently employ molecular dynamics (MD) simulations comparing the structures of Vv-DHDPS in the absence (PDB ID 3TUU) and presence of lysine (PDB ID 4HNN). These structural and computational studies reveal a significant rotation of Tyr132 suggesting binding of lysine attenuates the function of this catalytic triad residue. Our results offer significant insight into the allosteric regulation of an important plant enzyme.



## Materials and methods

### Cloning, expression and purification of Vv-DHDPS

The *dapA* gene encoding DHDPS from *V. vinifera* was purchased from Genentech and cloned into the pET28a expression vector as described elsewhere (Atkinson et al. 2011). Recombinant protein was produced in the host strain *E. coli* BL21-DE3 via induction by IPTG at 16 °C as described previously (Atkinson et al. 2011). Briefly, cells were harvested after an overnight induction (1 mM IPTG) and resuspended in 20 mM Tris–HCl, pH 8.0, 500 mM NaCl, 20 mM imidazole prior to lysis by sonication. Vv-DHDPS was subsequently isolated by metal-affinity liquid chromatography as described elsewhere (Atkinson et al. 2011).

### DHDPS-DHDPR coupled enzyme kinetic assay

Kinetic analyses of Vv-DHDPS were performed using the DHDPS-DHDPR coupled assay as described elsewhere (Dobson et al. 2004), using *E. coli* DHDPR as the coupling enzyme. Assays were routinely performed in triplicate at a constant temperature of 30 °C with reaction mixtures allowed to equilibrate in a temperature-controlled Cary 4000 UV–visible spectrophotometer for 10 min before initiating the reaction with 60 nM DHDPS. Prior to conducting kinetic measurements, pyruvate and ASA concentrations were quantified by the addition of limiting amounts of substrate and measuring the oxidation of NADPH spectrophotometrically at 340 nm. Initial rate data were analyzed using the ENZFITTER program available from Biosoft. Data were fitted to appropriate models as judged by Sigma values and the lowest standard error associated with the kinetic constants. Initial velocity data were fitted to the ping-pong model (1), mixed inhibition model (2), or non-competitive inhibition model (3), where appropriate, using the following kinetic equations:

$$v = V_{AB} / (K_{MB}A + K_{MA}B + AB) \quad (1)$$

$$v = VA / (\{K_m^{app}(1 + (I/K_i)^{n_{ES}})\} + \{A(1 + (I/K_i)^{n_E})\}) \quad (2)$$

$$v = VA / \{(1 + (I/K_i)^{n_{ES}})(K_m^{app} + A)\} \quad (3)$$

Here  $V$  is the maximal velocity,  $A$  and  $B$  are the substrate concentrations,  $K_{MA}$  and  $K_{MB}$  are the Michaelis–Menten constants for each substrate, and  $v$  is the initial velocity.  $K_m^{app}$  is the apparent Michaelis–Menten constant in models (2) and (3), while  $K_i$  and  $K_i'$  are the inhibition constants for  $I$  binding to the ES and E complex, respectively.  $n_{ES}$  and  $n_E$  are the Hill coefficient for  $I$  binding to the ES and E complex, respectively.

Hill equation Hill equation (Hill 1910):

$$\log(v/V - v) = -\log(I) - \log K_d$$

### Isothermal titration microcalorimetry

Calorimetric experiments were conducted using an ITC instrument (VP-ITC, MicroCal Inc, Northampton, MA, USA) using methods based on those outlined by Turnbull and Daranas (2003). Prior to ITC experiments, protein samples were exchanged into ITC buffer (200 mM HEPES, 5 mM pyruvate, pH 7.7) by overnight dialysis. A portion of the buffer was retained for flushing the instrument, blank measurements, and preparation of solutions containing ligand. All experiments were conducted at 20 °C and solutions were degassed under vacuum prior to use. A typical 35-injection protocol employed titrating ligand into Vv-DHDPS (initial concentration of 80 μM) protein solution using the following parameters:  $1 \times 10 \mu\text{L}$ , then  $34 \times 12 \mu\text{L}$  at 180 s intervals, using a syringe rotating at 310 rpm. The concentrations of ligands used were 2.5 and 10 mM lysine which was made up in the stock ITC buffer solution. Heats of dilution determined in the absence of protein were subtracted from the titration data prior to curve fitting. Additionally, the initial 10 μL injection was discarded from each dataset in order to remove the effect of titrant diffusion across the syringe tip during the equilibration process. Curve fitting was undertaken in Origin version 7.0 (OriginLab Corporation, Northampton, MA, USA) using the fitting algorithms supplied by MicroCal.

### CD spectroscopy

Circular dichroism (CD) spectra of Vv-DHDPS (4 μM) were recorded using an Aviv Model 410-SF CD spectrometer. Wavelength scans were performed between 198 and 250 nm in 20 mM Tris, 150 mM NaCl, pH 8.0 in 1.0 mm quartz cuvette as reported previously (Davis et al. 2004; Burgess et al. 2008; Voss et al. 2010). Data were analysed using the CDSSTR algorithm from the CDPro software package (Sreerama and Woody 2000; Davis et al. 2004) incorporating the SP22X protein database. For thermal denaturation scans, ellipticity at 222 nm was monitored between 20 and 90 °C in 1 °C steps.

### Analytical ultracentrifugation

Sedimentation velocity experiments were performed in a Beckman Coulter model XL-I analytical ultracentrifuge using similar methods to that reported previously (Atkinson et al. 2012; Burgess et al. 2008; Perugini et al. 2000; Voss et al. 2010). Double sector quartz cells were loaded with 400 μL of buffer and 380 μL of Vv-DHDPS at an initial

concentration of 13  $\mu\text{M}$ . The cells were loaded into an An50-Ti rotor and left to equilibrate at 30 °C. A rotor speed of 40,000 rpm was employed and absorbance readings were collected continuously at 280 nm (30 °C) using a step size of 0.003 cm without averaging. Initial scans were carried out at 3,000 rpm to determine the optimal wavelength and radial positions for the high speed experiment. Samples of Vv-DHDPS monitored in the presence of 1.0 mM lysine contained ligand in both the reference and sample channels. Solvent density, solvent viscosity, and estimates of the partial specific volume of Vv-DHDPS (0.7386 mL/g) at 30 °C were calculated using SEDNTERP (Laue et al. 1992). Data were analyzed via the ULTRASCAN software package (Demeler and van Holde 2004; Demeler 2005a, b), which can be downloaded from [www.ultrascan.uthscsa.edu](http://www.ultrascan.uthscsa.edu).

#### Crystallization of Vv-DHDPS and X-ray diffraction data

Initial crystallization trials were performed as previously described (Atkinson et al. 2011) using droplets consisting of 150 nL protein solution (in the presence of 20 mM pyruvate and 20 mM lysine) and 150 nL reservoir solution. Initial hit conditions were up scaled using the hanging-drop vapor-diffusion method with drops consisting of protein solution (2  $\mu\text{L}$ ) and precipitant solution (2  $\mu\text{L}$ ) at 20 °C. As noted with crystals grown in the presence of pyruvate alone (Atkinson et al. 2011), crystal growth in the presence of pyruvate and lysine required the precipitant concentration to be halved and protein concentration reduced to 2.5 mg/mL. A variety of crystal forms were observed from a number of different conditions. The best diffracting crystal (Supplementary Fig. 6a, b) grew from a modified version of condition 22 (0.1 M MES pH 6.5, 6 % (v/v) PEG 20,000), Hampton Research Crystal Screen 2. For X-ray data collection, a single crystal was transferred to a reservoir solution containing 20 % (v/v) glycerol and directly flash frozen in liquid nitrogen. Intensity data were collected at −163 °C at the Australian Synchrotron on the MX2 beamline (Evans and Pettifer 2001; McPhillips et al. 2002) using X-rays with a wavelength of 0.9536 nm. Data was collected in 0.5° steps with an exposure time of 2 s for one 360° pass, using an ADSC Q310r CCD detector positioned 280 mm from the crystal. Diffraction data sets were processed and scaled using the package MOSFLM (Leslie and Powell 2007) and SCALA (Collaborative Computational Project 1994; Evans 2006). Molecular replacement was performed using PHASER (McCoy et al. 2007) with pyruvate-bound Vv-DHDPS (PDB ID: 3TUU (Atkinson et al. 2012)) as the search model. Structural refinement of the resulting eight monomers in the asymmetric unit was performed using REFMAC5 (Collaborative

Computational Project 1994; Murshudov et al. 1997) with iterative model building using COOT (Emsley and Cowtan 2004). In the first steps of refinement, non-crystallographic restraints were applied, followed by simulated annealing using PHENIX (Adams et al. 2010). The structure was validated using the MolProbity Server (Chen et al. 2010). Refinement statistics are presented in Table 3. Ramachandran statistics showed 98.2 % of the residues in the most favored region, 1.5 % in the additionally allowed regions and 0.5 % (a single residue) in the disallowed region, namely Tyr 132, which is consistent with the equivalent Tyr residues observed in DHDPS structures from other species (Dobson et al. 2005b; Blagova et al. 2006).

#### Molecular dynamics simulations

Two independent molecular dynamics simulations were performed using tetrameric structures of Vv-DHDPS in the presence (PDB ID: 4HNN) and absence (PDB ID: 3TUU) of lysine. Residues outside the range 21–327 were removed from starting structures and the substrate, pyruvate, was removed from Lys184. Structures were solvated using the TIP3P water model in a rhombic dodecahedral shaped periodic box. The net charge of the simulation box was set to zero through the addition of sodium ions and additional ions were added to give an ionic concentration of 150 mM NaCl. The CHARMM force field (MacKerell et al. 1998) and the molecular dynamics package NAMD (Phillips et al. 2005) were used. Trajectories of 150 ns were generated at a constant temperature of 20 °C and atmospheric pressure. Snapshots of the full system were taken at 0.01 ns intervals and stored for analysis using VMD (Humphrey et al. 1996). Clustering of results was performed on a concatenated trajectory that contained a tight dimer pair from both the simulations. The clustering tool available in VMD was used with an RMSD based cutoff.

## Results and discussion

#### Vv-DHDPS is tightly inhibited by lysine

To characterize the kinetic properties of Vv-DHDPS, the coupled enzyme assay utilizing *E. coli* dihydrodipicolinate reductase (DHDPR, Fig. 2) as the coupling enzyme (Dobson et al. 2004) was performed at varying lysine and substrate (i.e. pyruvate and ASA) concentrations. Figure 3a shows plots of initial velocity as a function of lysine and pyruvate concentrations. The plots reveal a sigmoidal relationship that is characteristic of cooperative allosteric enzyme inhibition (Cornish-Bowden 1976). The equivalent kinetics data determined at varying ASA concentrations are

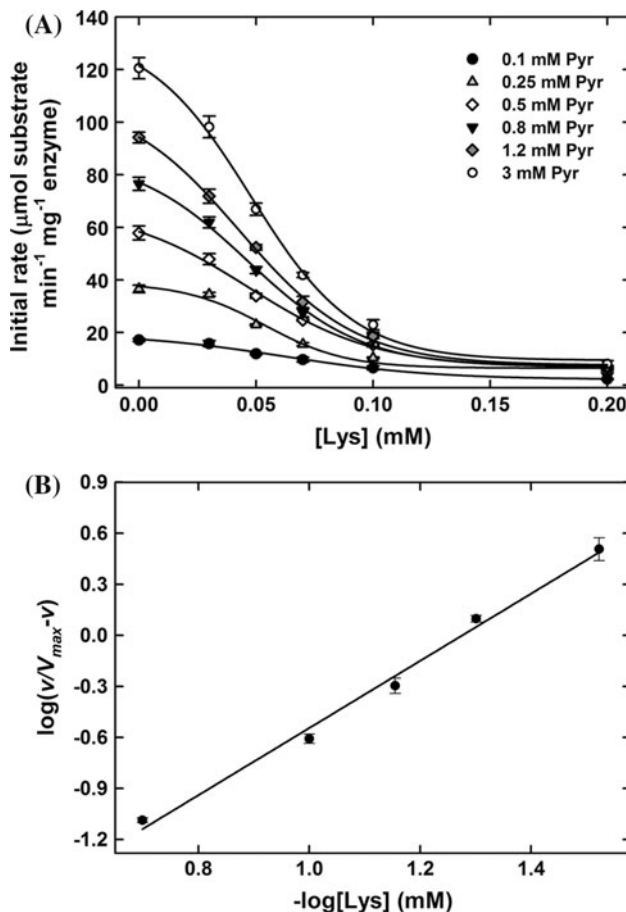


**Fig. 3** Lysine inhibition of Vv-DHDPS. **a** Kinetic analyses were performed by measuring the initial velocity of Vv-DHDPS with respect to various concentrations of the substrate pyruvate (Pyr) and inhibitor lysine (Lys). Initial velocity data were fitted to a mixed inhibition kinetic model (Eq. 2) using ENZFITTER (Biosoft software). Each data point was measured in triplicate. **b** Hill plot using data collected at a fixed Pyr concentration of 1.2 mM yielding a slope (apparent Hill coefficient,  $n_{app}$ ) of 1.9 (Table 1)

plotted in Supplementary Fig. 1a. Subsequent Hill plots were generated to provide estimates of the Hill coefficient ( $n_{app}$ ). This yielded  $n_{app}$  of 1.9 with respect to pyruvate (Fig. 3b) and 1.7 with respect to ASA (Supplementary Fig. 1b). The data indicates positive cooperativity and suggests that the binding of one lysine molecule increases the affinity of the enzyme for additional molecules (Cornish-Bowden 1976).

The mode of lysine inhibition with respect to both substrates was next investigated. The effect of increasing lysine concentrations at either (1) fixed pyruvate concentration (5 mM) and varied ASA concentrations or (2) fixed ASA (1.2 mM) and varied pyruvate concentrations was examined. In both cases, the double reciprocal plots (Supplementary Fig. 2) intersected to the left of the 1/V axis indicating both  $K_M$  and  $V_{max}$  are affected by the presence of lysine. This is characteristic of mixed

**Table 1** Kinetic properties of Vv-DHDPS

<i>With respect to pyruvate (Pyr)</i>	
$K_I^{LYS}$ (Pyr)	$K_I^{LYS}$ (ES) = $0.063 \pm 0.02$ mM $K_I^{LYS}$ (E) = $0.054 \pm 0.01$ mM
Apparent Hill coefficient ( $n_{app}$ ) <sup>a</sup>	1.9
$n_{ES}/n_E$	$1.0 \pm 0.1/2.4 \pm 0.3$
<i>With respect to ASA</i>	
$K_I^{LYS}$ (ASA)	$0.049 \pm 0.01$ mM
Apparent Hill coefficient ( $n_{app}$ ) <sup>c</sup>	1.7
Hill coefficient ( $n$ ) <sup>d</sup>	$1.7 \pm 0.2$

<sup>a</sup> Apparent Hill coefficient determined from Fig. 3b

<sup>b</sup> Hill coefficients derived from the nonlinear best fit to a mixed inhibition model (Fig. 3a)

<sup>c</sup> Apparent Hill coefficient determined from Supplementary Fig. 1b

<sup>d</sup> Hill coefficients derived from the nonlinear best fit to a mixed (non-competitive) inhibition model (Supplementary Fig. 1a)

inhibition, indicating that lysine binds to free DHDPS and also the DHDPS-substrate complex (Supplementary Fig. 2). Fitting the data to a mixed inhibition model revealed  $K_{i(ES)} = 0.063$  mM and  $K_{i(E)} = 0.054$  mM with respect to pyruvate, suggesting a slightly lower affinity for the DHDPS-pyruvate complex compared to the free enzyme (Fig. 3a; Table 1). The resulting Hill coefficients were 1.0 and 2.4 for  $n_{ES}$  and  $n_E$ , respectively (Table 1). With respect to ASA, lysine is a noncompetitive inhibitor (affinity for E and ES is the same) with a single  $K_i$  of 0.049 mM and  $n$  of 1.7 (Supplementary Fig. 1a; Table 1).  $K_i$  values for lysine of less than 0.1 mM are consistent with that observed for DHDPS from other plant species, including *T. aestivum* (Kumpaisal et al. 1987), *D. carota sativa* (Matthews and Widholm 1979), *S. oleracea* (Wallsgrove and Mazelis 1980), *Z. mays* (Frisch et al. 1991) and *P. sativum* (Dereppe et al. 1992) and are significantly tighter than those typically observed for DHDPS from Gram-negative bacteria (Yugari and Gilvarg 1965; Devenish et al. 2009; Soares da Costa et al. 2010).

To verify the cooperativity observed in the enzyme kinetic data and determine accurate lysine binding affinities at equilibrium, the thermodynamics of lysine binding to Vv-DHDPS was measured by isothermal titration microcalorimetry (ITC) in the presence of saturating pyruvate. Titration of 80 μM Vv-DHDPS with 10 mM lysine (Supplementary Fig. 3a) and 2.5 mM lysine (Supplementary Fig. 3b) generated isotherms diagnostic of cooperative binding, in which ligand addition initially results in increasing heat of association, followed by binding site saturation (Bradrick et al. 1996; Phenix and Palmer 2008). As the two lysine molecules occupy symmetry-related binding sites within the allosteric cleft, the binding isotherm was fitted to a sequential binding site model, as described previously (Muscroft-Taylor et al. 2010). The

**Table 2** Thermodynamic parameters determined by ITC<sup>a</sup>

$K_d(\text{Lys}_1)$ (mM)	$0.002 \pm 0.0003$
$\Delta H_1$ (kJ/mol)	$-81 \pm 6.2$
$T\Delta S_1$ (kJ/mol)	600
$K_d(\text{Lys}_2)$ (mM)	$0.38 \pm 0.14$
$\Delta H_2$ (kJ/mol)	$-870 \pm 27$
$T\Delta S_2$ (kJ/mol)	340

<sup>a</sup> Experiments were performed by titrating lysine into Vv-DHDPS (initial concentration = 80  $\mu\text{M}$ ) at 20 °C in 200 mM HEPES 5 mM pyruvate, pH 7.7. Best fits were obtained by employing a sequential two site model

resulting thermodynamic parameters are presented in Table 2. Interaction of the first lysine ( $\text{Lys}_1$ ) with the binding site was characterized by an affinity of 2  $\mu\text{M}$  comprised primarily of an entropic effect with a small enthalpic contribution (Table 2). By contrast, the second binding interaction ( $\text{Lys}_2$ ) is 190-fold weaker in affinity, but has a significantly greater enthalpic contribution with a reduced entropic component (Table 2). This appears to be a case of enthalpy-driven positive cooperativity (Ricard and Cornish-Bowden 1987), which is consistent with previous ITC studies of *E. coli* DHDPS titrated with lysine (Muscroft-Taylor et al. 2010). However, the affinities of Vv-DHDPS for lysine are significantly tighter than the *E. coli* enzyme. In contrast, ITC studies show that the binding energy of MosA for lysine was characterized as primarily entropic for both sites, in which the second site contributed >90 % of the interaction energy (Phenix and Palmer 2008).

Pyruvate and lysine significantly stabilize the secondary structure of Vv-DHDPS

Recent studies show that the thermostability of bacterial DHDPS enzymes is significantly enhanced in the presence of pyruvate, which is the first substrate to bind the enzyme (Burgess et al. 2008; Domigan et al. 2009; Voss et al. 2010). However, no change in thermostability is observed in the presence of ASA, the second substrate to bind in the DHDPS-catalysed reaction (Burgess et al. 2008; Voss et al. 2010). By contrast, the effect of lysine on the thermostability of plant DHDPS has not yet been reported. To assess if lysine influences the thermostability of Vv-DHDPS in solution, circular dichroism (CD) spectroscopy studies were conducted. Initially, wavelength scans were measured at 20 °C to compare the global secondary structure of Vv-DHDPS in the absence and presence of ligand. This revealed no significant change in secondary structure upon addition of saturating amounts of pyruvate or lysine (Supplementary Fig. 4). Thermal denaturation experiments were subsequently performed in the presence and absence

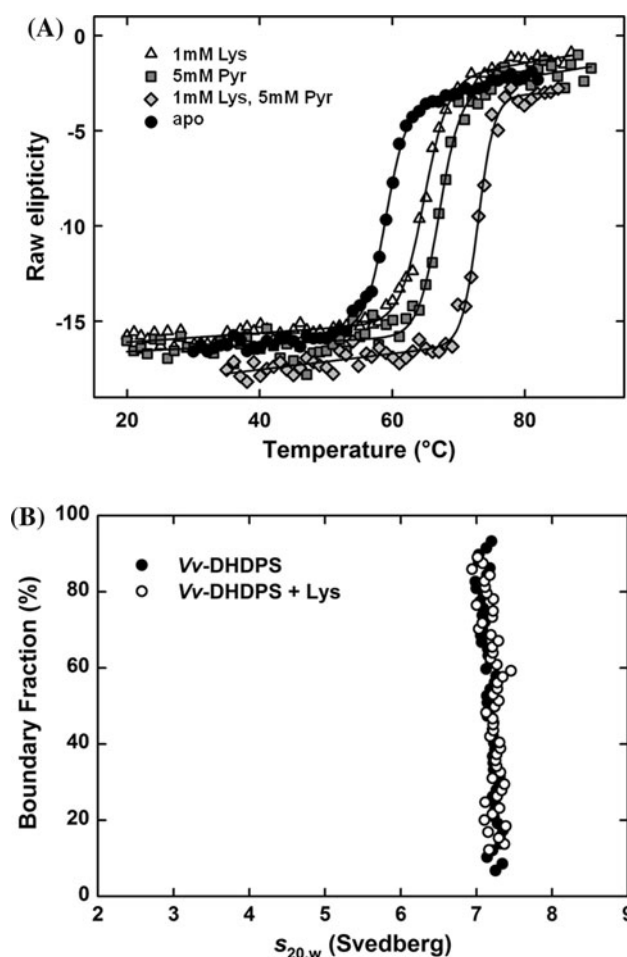


**Fig. 4** Thermostability and quaternary structure of Vv-DHDPS in the absence and presence of lysine. **a** Thermal denaturation of unliganded (*apo*) Vv-DHDPS (filled circle), enzyme in the presence of; 2.0 mM pyruvate (Pyr) (open square), 0.5 mM lysine (Lys) (open triangle) and 5 mM pyruvate & 1 mM lysine (open diamond). **b** Enhanced van Holde-Weischet integral distribution plot from extrapolation of Vv-DHDPS raw sedimentation velocity data shown in Supplementary Fig. 4. The corrected sedimentation coefficient is plotted against the boundary fraction for Vv-DHDPS (13  $\mu\text{M}$ ) in the absence (filled circle) and presence (open circle) of 1.0 mM lysine (Lys)

of saturating concentrations of ligands over the temperature range of 20–90 °C (Fig. 4a). Vv-DHDPS appears to follow a two-state mechanism for thermal unfolding in the absence of ligands, with an apparent melting temperature of 59.0 °C (Fig. 4a). However, in the presence of 5.0 mM pyruvate or 1.0 mM lysine, the thermal denaturation of Vv-DHDPS is delayed with respect to temperature, with apparent melting temperature increasing significantly to 67.1 and 64.7 °C, respectively. Interestingly, the presence of both ligands markedly accentuates the thermostability of the enzyme with the apparent melting temperature increasing to 73.0 °C (Fig. 4a). Although no secondary structural changes were observed in the presence of



ligands, the significant increase in thermostability in the presence of pyruvate and/or lysine may be associated with changes in tertiary and/or quaternary structure. Indeed, pyruvate has previously been shown to stabilize the quaternary structure of bacterial DHDPS enzymes (Burgess et al. 2008; Voss et al. 2010), but to date, there have been no studies demonstrating the effect of lysine on the quaternary structure of DHDPS.

Lysine does not change the quaternary structure of *Vv*-DHDPS in solution

To determine if lysine influences the quaternary structure of *Vv*-DHDPS, sedimentation velocity experiments were conducted in the analytical ultracentrifuge. Interestingly, recent studies show that dimeric mutants of bacterial DHDPS possess significantly attenuated catalytic function compared to their wild-type tetrameric counterparts (Griffin et al. 2008, 2010; Voss et al. 2010). It is thus possible, that lysine mediates allosteric inhibition by inducing dissociation of the *Vv*-DHDPS tetramer (Fig. 1b) into less active dimers that are nonetheless more thermostable. However, in both the absence and presence of lysine, the absorbance versus radial position profiles of *Vv*-DHDPS show a single sedimenting boundary whose rate of movement appears unchanged upon addition of ligand suggesting there is no change in quaternary structure (Supplementary Fig. 5). This assertion is supported by analyzing the data in a model-independent manner using the enhanced van Holde-Weischet method employing the ULTRASCAN software suite (Demeler and van Holde 2004; Demeler 2005a, b). As shown in Fig. 4b, the resultant distributions show that *Vv*-DHDPS in the presence or absence of lysine exists as a single 7.2 S species, which correlates to the tetrameric form (Fig. 1b) (Atkinson et al. 2012). This verified that the quaternary structure of *Vv*-DHDPS remains unchanged in the presence of lysine, suggesting that lysine-enhanced thermostability is mediated through changes in tertiary structure.

Structure of *Vv*-DHDPS in complex with lysine reveals a conformational change

Given that lysine enhances enzyme thermostability but does not alter the secondary or quaternary structure of *Vv*-DHDPS, we next set out to examine the tertiary structural changes, if any, accompanying binding of the allosteric inhibitor. As described previously (Atkinson et al. 2011), attempts to crystallize *Vv*-DHDPS in the absence of ligand were unsuccessful, but the addition of pyruvate resulted in crystal formation, although in-drop thrombin cleavage was required to generate diffracting crystals. Crystal trials in the presence of both pyruvate and lysine were much more

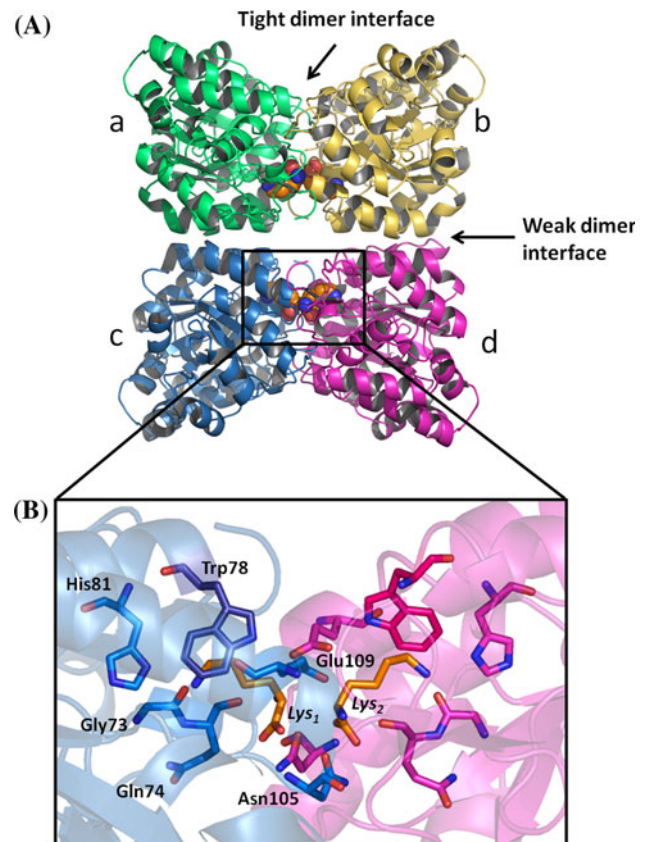


**Fig. 5** Crystal structure of *Vv*-DHDPS bound to lysine. **a** Crystal structure of *Vv*-DHDPS (PDB ID: 4HNN) showing the position of inhibitory lysine molecules (orange spheres) in each allosteric site and the self-association interfaces. Two monomers come together at the tight dimer interface to form the dimeric unit, which dock at the weak dimer interface to form a homotetramer. The asymmetric unit contained eight monomers assembled as two homotetramers. **b** Allosteric site residues of *Vv*-DHDPS. Two bound lysine molecules (*Lys*<sub>1</sub> and *Lys*<sub>2</sub>) are indicated (orange)

successful, with several conditions producing large crystals without the need for in-drop thrombin cleavage. The best diffracting crystal (Supplementary Fig. 6a, b) was cultivated from a modified version of condition 22 of Hampton Research Crystal Screen 2 (reservoir solution: 0.1 M MES pH 6.5, 6 % (v/v) PEG 20,000). This result correlates with solution-based studies of *Vv*-DHDPS described above, where the addition of both pyruvate and lysine significantly increase the thermostability of the enzyme (Fig. 4a).

The crystal structure of *Vv*-DHDPS in the presence of pyruvate & lysine was determined by molecular replacement using pyruvate-bound *Vv*-DHDPS (PDB ID 3TUU) as the search model (Fig. 1b). The structure (PDB ID 4HNN) revealed two tetramers of *Vv*-DHDPS in the asymmetric unit, both displaying a ‘back to back’ quaternary architecture (Fig. 5a) as previously observed for DHDPS from *N. sylvestris* (Blickling et al. 1997a), *A. thaliana* (Griffin et al. 2012) and the pyruvate-bound structure from *V.*

**Table 3** Data collection, processing and refinement statistics for Vv-DHDPS (PDB ID: 4HNN)

Wavelength (Å)	0.9536
No. of images	360
Step range (°)	0.5
Space group	C2
Unit cell parameters (Å)	a = 220.6, b = 137.9, c = 133.9
Bond angles (°)	$\alpha = \gamma = 90.0$ , $\beta = 108.0$
Resolution (Å)	52.4–2.40 (2.53–2.40)
Observed reflections	362,734 (53663)
Unique reflections	146,233 (21393)
Completeness (%)	98.5 (99.0)
$R_{\text{merge}}^a$	0.101 (0.412)
$R_{\text{r.i.m}}^b$	0.124 (0.505)
$R_{\text{p.i.m}}^c$	0.072 (0.288)
Mean I/ $\sigma$ (I)	9.8 (2.7)
Redundancy	2.5 (2.5)
Wilson B value	24.4
Molecules per ASU	8
$V_M$ (Matthews coefficient)	2.30
Solvent content (%)	47
$R_{\text{cryst}}$	18.4
$R_{\text{free}}$	22.0
<i>Number of atoms</i>	
Protein	19,233
Water	1,083
<i>R.m.s.d.</i>	
Bonds	0.01
Angles	1.20
<i>Average B factors</i>	
Protein	24.0
Water	27.7
<i>Ramachandran plot, # residues (%)</i>	
Favored region	98.2
Allowed region	1.5
Disallowed region	0.3

Values in parentheses are for the highest resolution bin

$$^a R_{\text{merge}} = \sum_{hkl} \sum_i |I_i(hkl) - \langle I(hkl) \rangle| / \sum_{hkl} \sum_i I_i(hkl)$$

$$^b R_{\text{r.i.m}} = \sum_{hkl} [N/(N-1)]^{1/2} \sum_i |I_i(hkl) - \langle I(hkl) \rangle| / \sum_{hkl} \sum_i I_i(hkl)$$

$$^c R_{\text{pim}} = \sum_{hkl} [1/(N-1)]^{1/2} \sum_i |I_i(hkl) - \langle I(hkl) \rangle| / \sum_{hkl} \sum_i I_i(hkl)$$

where  $I_i(hkl)$  is the  $i$ th intensity measurement of reflection  $hkl$  and  $\langle I(hkl) \rangle$  its average and  $N$  is the redundancy of a given reflection

*vinifera* (Atkinson et al. 2012) (Fig. 1b). The r.m.s.d. between the two tetramers is 2.9 Å. The final molecule had an overall  $R_{\text{cryst}}$  of 18.4 % ( $R_{\text{free}}$  of 22.0 %) to 2.4 Å resolution. The 4HNN model was also examined using the MolProbity server (Chen et al. 2010), which revealed that 98.2 % of residues in Vv-DHDPS bound to lysine and pyruvate were located in the favored regions of the Ramachandran plot. The eight residues in the ‘disallowed’

regions correspond to the catalytic site residue Tyr132 from each of the eight chains. This is not unexpected as this highly conserved residue has been shown to reside in the disallowed region of the Ramachandran plot in all other DHDPS structures determined to date (Mirwaldt et al. 1995; Dobson et al. 2005b, 2008; Blagova et al. 2006; Burgess et al. 2008; Devenish et al. 2008; Girish et al. 2008; Kefala et al. 2008; Voss et al. 2010; Atkinson et al.

2012). A summary of the crystallographic data collection and refinement statistics is provided in Table 3.

The structure shows that each monomer is comprised of an N-terminal ( $\beta/\alpha$ )<sub>8</sub>-barrel domain and a C-terminal domain consisting of 3  $\alpha$ -helices and 2 short  $\beta$ -strands (Supplementary Fig. 7a). As for the pyruvate-bound structure (PDB ID 3TUU) (Atkinson et al. 2012), the N terminus of each monomer is absent from the observed electron density, presumed to be mostly disordered. Owing to the crystallization conditions used, electron density associated with pyruvate is found covalently bound to the active site lysine (Lys184) in each subunit. The active site forms around this key lysine residue, which is located at the center of each monomeric unit (Supplementary Fig. 7b). The spatial orientation of the three conserved catalytic triad residues, namely Tyr132, Thr69 and Tyr156, as well as Arg161 and Ile223 that are also important for catalytic activity, is consistent with that observed in the active sites of other DHDPS structures (Dobson et al. 2004, 2005a, 2008).

Following the first round of refinement, electron density was observed at the tight dimer interfaces of both tetramers, which was not accounted for by the search model (PDB ID 3TUU). Subsequent manual modeling of this density supports the occupancy of two lysine molecules bound in the allosteric pocket at the interface of the tight dimer (i.e. interface ab or cd, Fig. 5a) and in weak contact with each other (3.5 Å between alpha carbons) (Fig. 5b). Following final refinement, an omit map was generated, confirming the presence and orientation of the lysine molecules (Supplementary Fig. 8). The refined structure shows that the carboxyl group of lysine is coordinated by the hydroxyl group of Tyr131 and the amide of the Asn105 of the adjacent subunit. Importantly, the  $\alpha$ -amino group forms a salt bridge with Glu109 and a hydrogen bond with Asn105, as well as a hydrogen bond with Gln74 (Fig. 5b). Since crystals were generated at pH 6.5, the amino group of lysine would be in a protonated state and thus able to form a salt bridge. The  $\epsilon$ -amino group is coordinated by Trp78, His81 and a hydrogen bond with the main-chain oxygen atom of Gly73 (Fig. 5b). Additional van der Waals contacts are formed with Met76, Ser77, Asn101, Gly103, Ser104, Ser106 and Tyr132, completing the allosteric site.

As stated earlier, a range of transgenic plants have been generated in which point-mutations targeting DHDPS have abolished lysine inhibition (Frankard et al. 1992; Perl et al. 1992; Shaul and Galili 1992a; Galili 1995; Ghislain et al. 1995; Kwon et al. 1995; Bittel et al. 1996; Brinch-Pedersen et al. 1996; Silk and Matthews 1997). For instance, Trp78Arg (Vauterin et al. 2000), Asn105Ile (Ghislain et al. 1995), Ser104Asn (Shaver et al. 1996) and Glu109Lys (Shaver et al. 1996) (*Vv*-DHDPS numbering) substitutions

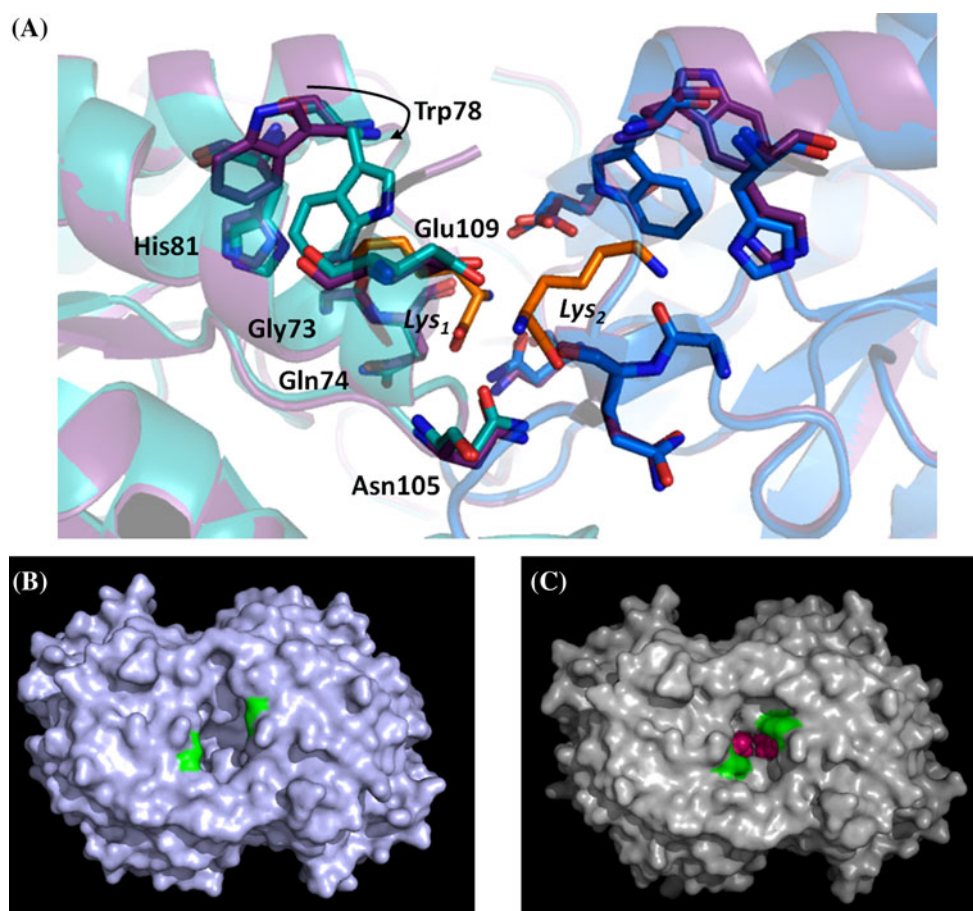
in DHDPS from a number of plant species have resulted in enzymes that are not regulated by lysine. Our study of *Vv*-DHDPS shows that these residues are important for stabilizing allosteric interactions. Interestingly, an Ala113Val substitution (Bittel et al. 1996; Shaver et al. 1996; Silk and Matthews 1997) has also resulted in lysine-insensitivity. The reason for this is at first unclear, given that Ala113 does not appear to make contacts with lysine bound in the allosteric cleft. However, close inspection of the allosteric site reveals the close proximity of Ala113 to Trp78, and thus it is likely that a valine substitution displaces Trp78 interfering with lysine binding.

Both the pyruvate & lysine bound (Fig. 5a) and the previously reported pyruvate-bound (Fig. 1b) (Atkinson et al. 2012) structures of *Vv*-DHDPS are very similar. The backbone of the two tetramers align with an r.m.s.d. of 0.34 Å with no significant differences observed in the key active site residues (Supplementary Fig. 7b). However, it is noted that Trp78 in the allosteric cleft moves significantly upon lysine binding (Fig. 6a, Supplementary Fig. 9a). This residue acts as a lid, greatly reducing the solvent accessibility of the allosteric site once lysine is bound (Fig. 6b, c). This movement, together with a rearrangement of residues His81 (Supplementary Fig. 9b) and Ile82, is similar to that seen in *N. sylvestris* DHDPS (Blickling et al. 1997a). Notably, however, the small displacement of helix  $\alpha$ 2 towards the inhibitor binding pocket observed in *N. sylvestris* DHDPS upon lysine binding (Blickling et al. 1997a) is not apparent in *Vv*-DHDPS. Likewise, rearrangement of the tight-dimer units in *N. sylvestris* DHDPS upon lysine binding (Blickling et al. 1997a) is not observed for the *Vv*-DHDPS structure reported in this study.

Following lysine binding to *Vv*-DHDPS, the hydroxyl group of Tyr131 is drawn towards the carboxyl group of lysine, changing its position by  $0.69 \pm 0.09$  Å averaged across 8 monomers in the asymmetric unit (Supplementary Fig. 9c). Tyr131 forms a hydrophobic stack with the interdigitating catalytic triad residue, Tyr132, which is contributed by the adjacent monomer across the tight dimer interface (Supplementary Fig. 7b). The reorientation of Tyr131 upon lysine binding disrupts this packing, displacing the hydroxyl group of Tyr132 by  $0.56 \pm 0.05$  Å (Supplementary Fig. 9c). We propose this is sufficient to disrupt the function of the catalytic triad, which involves proton relay from pyruvate through the catalytic triad of Tyr156-Thr69-Tyr132 to solvent (Supplementary Fig. 7b) (Dobson et al. 2004). This suggests a potential structural mechanism for lysine-mediated allosteric inhibition through the abrogation of catalytic triad function.

In addition to elucidating significant differences in the orientation of key allosteric and active site residues, it was

**Fig. 6 a** Allosteric site residues are shown from structures derived from *Vv*-DHDPS in the absence (purple) and presence (blue) of inhibitory lysine molecules (orange). **b** Space fill representation of *Vv*-DHDPS looking onto the allosteric binding cleft in the absence of lysine. Trp78 is indicated in green. **c** Space fill representation of *Vv*-DHDPS looking onto the allosteric binding cleft in the presence of lysine (pink). Trp78 is shown in green. The binding pocket closes upon binding lysine



anticipated that the structure of *Vv*-DHDPS bound to lysine would also provide insight into the enhanced thermostability observed for the enzyme in the presence of lysine (Fig. 4a). Computational analyses using the Protein Interfaces, Surfaces and Assemblies (PISA) program available on the European Bioinformatics Institute website (Krissinel and Henrick 2007) show that the total solvent inaccessible surface area (SISA) at the ‘tight’ dimer interface of lysine-bound *Vv*-DHDPS is 1827 Å<sup>2</sup> compared to 1788 Å<sup>2</sup> at the equivalent interface of the *Vv*-DHDPS structure in the absence of lysine (Supplementary Table 1). The larger buried surface area is due to a greater number of residues comprising this interface. Of note, two additional residues contribute to hydrogen bond formation, whilst one additional residue contributes to an ion–ion interaction across this interface (Supplementary Table 1). Together, the increase in SISA and additional contacts would explain the increased stability observed in thermal denaturation studies (Fig. 4a). By contrast, minor differences exist between the two structures at the weak dimer interface with a slight reduction in SISA, but a subtle increase in the total number of noncovalent interactions upon lysine binding (Supplementary Table 1).

#### Comparison of plant and bacteria allosteric sites

It has been observed that the  $K_i$  for lysine inhibition in plant DHDPS is often up to 20-fold tighter than that observed in bacterial DHDPS enzymes (Yugari and Gilvarg 1965; Webster and Lechowich 1970; Yamakura et al. 1974; Hoganson and Stahly 1975; Halling and Stahly 1976; Matthews and Widholm 1979; Kumpaisal et al. 1987; Cremer et al. 1988; Frankard et al. 1992; Shaul and Galili 1992b; Cahyanto et al. 2006; Burgess et al. 2008; Devenish et al. 2009; Domigan et al. 2009; Soares da Costa et al. 2010). To better understand the nature of this difference, the allosteric site of *Vv*-DHDPS was compared to the equivalent site in the structure of *E. coli* DHDPS bound to lysine (PDB ID: 1YXD) (Dobson et al. 2005b) (Supplementary Fig. 10). Many residues that make up the allosteric site of *E. coli* DHDPS (Dobson et al. 2005b) are conserved in *Vv*-DHDPS, including Asn105, Glu109 and His81 (*Vv*-DHDPS numbering). However, the plant binding cleft is narrower than the equivalent site in bacteria with the distance between adjacent lysine molecules spanning 3.5 Å in *Vv*-DHDPS compared to 4.1 Å in *E. coli* DHDPS. Most importantly, bacterial DHDPS enzymes lack



an equivalent Trp78 residue. Instead, a histidine residue acts like a 'lid' upon lysine binding in the *E. coli* structure (Supplementary Fig. 10). This histidine residue lacks the steric bulk of a tryptophan, thus leaving the allosteric site much more exposed to solvent. In addition, whilst the allosteric site is located on the external surface of the molecule in *E. coli* DHDPS (Fig. 1a), the architecture of Vv-DHDPS means that the lysine binding site is located in the center of the tetramer in proximity to the adjacent dimer (Fig. 5a).

### Molecular dynamics simulations

To provide further insight into the mechanism of lysine-mediated allosteric inhibition, molecular dynamics (MD) simulations were performed on lysine-bound Vv-DHDPS

(PDB ID: 4HNN) compared to the lysine free enzyme (PDB ID: 3TUU). Figure 7 summarizes the MD simulation results. The root mean squared deviation of the tetramer (Fig. 7a) shows that the lysine bound form (red trajectory) is tighter than the unoccupied form (black trajectory) with a lower deviation from the crystal structure over the course of the 150 ns simulation. This is consistent with thermostability measurements in solution (Fig. 4a). The root mean squared fluctuation taken on a chain-by-chain basis shows a mixture of different fluctuations with no clear consensus that is dependent on the presence of lysine (Fig. 7a). However, changes in the dynamics of the catalytic triad can be observed particularly in the rotation of Tyr132 around the  $\chi_2$  dihedral angle (Fig. 7c). Although the crystal structure shows this key catalytic residue is displaced by 0.6 Å upon lysine binding (Supplementary Fig. 9c), MD

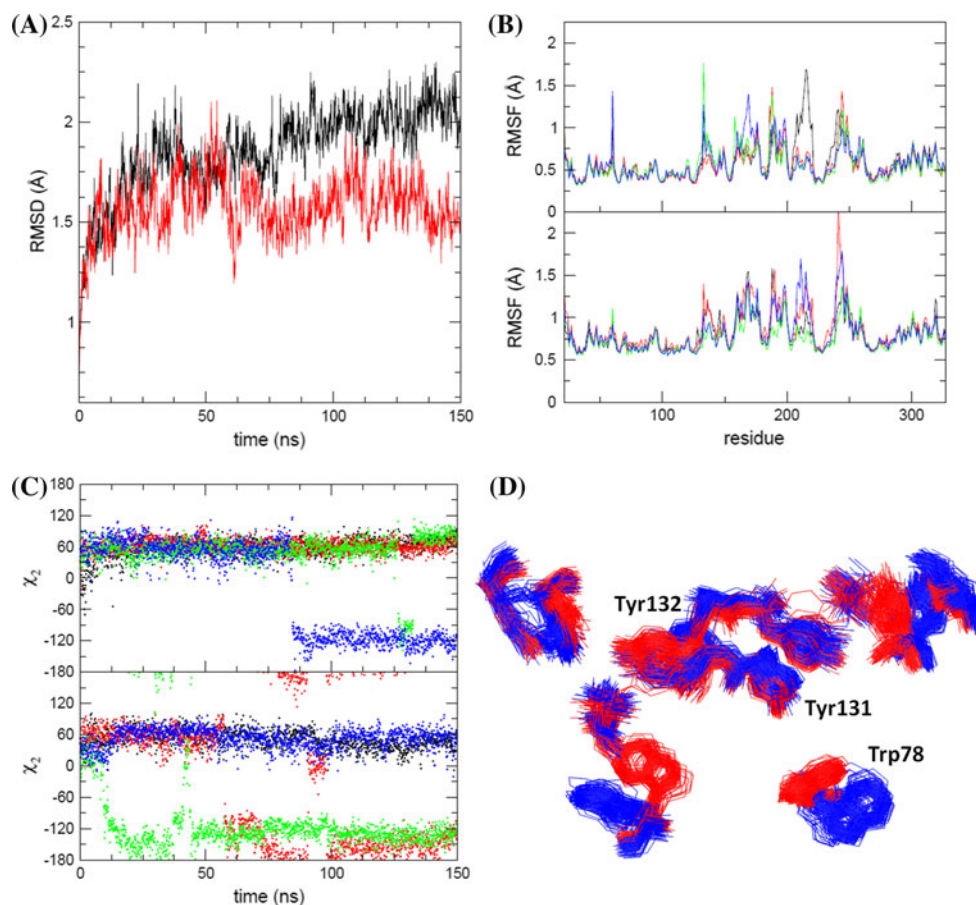


**Fig. 7** Molecular dynamics simulations. **a** Root mean squared deviation (*RMSD*) of the protein backbone for tetrameric Vv-DHDPS in the presence (*red*) and absence (*black*) of lysine. **b** Root mean squared fluctuation (*RMSF*) of the protein backbone on a chain-by-chain basis for lysine free (*upper panel*) and lysine bound (*lower panel*) MD simulations. Each *trace* represented in a different *color* is derived from separate monomers within tetrameric Vv-DHDPS. **c** Rotational motion of Tyr132 in the lysine free enzyme (*upper panel*) and lysine bound structure (*lower panel*) MD simulations as

measured by the  $\chi_2$  ( $C_{\alpha}-C_{\beta}-C_{\gamma}-C_{\delta 1}$ ) dihedral angle. Each *trace* presented in different *colors* is derived from separate monomers within tetrameric Vv-DHDPS. **d** Clustering of snapshots based on overall backbone conformation from a concatenated trajectory containing frames from both simulations. The clustering of snapshots was performed on one of the tight dimer units only with similar results found for the opposing tight dimer pair. Only the two most populated clusters are shown (*blue* 41 %; *red* 32 %). Displayed residues include Trp78, Tyr131 and Tyr132

simulations demonstrate lysine binding has a much more profound effect on the orientation and dynamics Tyr132. Analyses show that transitions between the equivalent orientations for Tyr132 happen infrequently during the 150 ns simulations for the unoccupied enzyme (Fig. 7c, upper panel), but relatively rapidly when lysine is bound to the allosteric site (Fig. 7c, lower panel). In addition, clustering of a mixed trajectory formed by concatenating tight-dimer trajectories from the lysine bound and lysine free simulations were performed (Fig. 7d). The clustering is based on the backbone conformation alone, but the two most occupied clusters discriminate between those structures that contain lysine in the allosteric site and those that do not, as seen by the orientation of Trp78 (Fig. 7d). These clusters contain quite different side chain orientations of key active and allosteric site residues, including Tyr132, when lysine is bound to the allosteric cleft. Overall, the MD simulation results show marked differences in the dynamics of key residues, particularly Tyr132, based on the occupancy of the lysine binding pocket. This supports the notion that the structural mechanism of lysine allosteric inhibition is mediated through enhanced dynamics and displacement of Tyr132, which results in inefficient catalytic triad function. Furthermore, this phenomenon explains why lysine is a partial inhibitor of DHDPS, since functional orientation of Tyr132 is still possible, but less likely in the presence of allosteric inhibitor.

## Conclusions

In conclusion, we show using enzyme kinetic and calorimetric studies in solution that dihydrodipicolinate synthase (DHDPS) from *V. vinifera* is allosterically inhibited by lysine in a cooperative manner with tenfold greater potency than that reported for bacterial orthologs. Although no change in secondary or quaternary structure is observed upon lysine binding, the allosteric inhibitor induces a significant increase in thermostability. This is manifested by conformational changes in key allosteric and active site residues, including Trp78, Tyr131 and Tyr132. MD simulations provide further insight showing that lysine binding leads to enhanced rotation of Tyr132, which we propose abrogates the function of the catalytic triad of Thr69, Tyr156 and Tyr132. Together, these findings provide valuable structural insights into the mechanism of lysine-mediated allosteric inhibition of DHDPS from an agriculturally-important plant species.

**Acknowledgments** We would firstly like to acknowledge the support and assistance of the friendly staff at the Bio21 Collaborative Crystallographic Centre at CSIRO Molecular and Health Technologies, Parkville, Melbourne and the beamline scientists at the Australian Synchrotron, Victoria, Australia. We would also like to thank

all members of the Perugini laboratory for helpful discussions during the preparation of this manuscript. Finally, we acknowledge the Australian Research Council for providing a Future Fellowship for M.A.P. and P.C. and the University of Melbourne (FRGSS 2011 Project grant) for project funding. R.C.J.D. acknowledges the CR Roper Bequest for Fellowship support. This research was supported by a Victorian Life Sciences Computation Initiative (VLSCI) grant number VR0089 on its Peak Computing Facility at the University of Melbourne, an initiative of the Victorian Government, Australia.

## References

- Adams PD, Afonine PV, Bunkoczi G, Chen VB, Davis IW, Echols N, Headd JJ, Hung LW, Kapral GJ, Grosse-Kunstleve RW, McCoy AJ, Moriarty NW, Oeffner R, Read RJ, Richardson DC, Richardson JS, Terwilliger TC, Zwart PH (2010) PHENIX: a comprehensive Python-based system for macromolecular structure solution. *Acta Crystallogr D Biol Crystallogr* 66:213–221
- Atkinson SC, Dogovski C, Newman J, Dobson RC, Perugini MA (2011) Cloning, expression, purification and crystallization of dihydrodipicolinate synthase from the grapevine *Vitis vinifera*. *Acta Crystallogr Sect F Struct Biol Cryst Commun* 67:1537–1541
- Atkinson SC, Dogovski C, Downton MT, Pearce FG, Reboul CF, Buckle AM, Gerrard JA, Dobson RCJ, Wagner J, Perugini MA (2012) Crystal, solution and in silico structural studies of dihydrodipicolinate synthase from the common grapevine. *PLoS One* 7:e38318
- Ben-Tzvi Tzchori I, Perl A, Galili G (1996) Lysine and threonine metabolism are subject to complex patterns of regulation in *Arabidopsis*. *Plant Mol Biol* 32:727–734
- Bittel D, Shaver J, Somers D, Gengenbach B (1996) Lysine accumulation in maize cell cultures transformed with a lysine-insensitive form of maize dihydrodipicolinate synthase. *Theor App Genet* 92:70–77
- Blagova E, Levdivkov V, Milioti N, Fogg MJ, Kalliomaa AK, Brannigan JA, Wilson KS, Wilkinson AJ (2006) Crystal structure of dihydrodipicolinate synthase (BA3935) from *Bacillus anthracis* at 1.94 Å resolution. *Proteins* 62:297–301
- Blickling S, Beisel HG, Bozic D, Knablein J, Laber B, Huber R (1997a) Structure of dihydrodipicolinate synthase of *Nicotiana sylvestris* reveals novel quaternary structure. *J Mol Biol* 274:608–621
- Blickling S, Renner C, Laber B, Pohlenz HD, Holak TA, Huber R (1997b) Reaction mechanism of *Escherichia coli* dihydrodipicolinate synthase investigated by X-ray crystallography and NMR spectroscopy. *Biochemistry* 36:24–33
- Boughton BA, Griffin MDW, O'Donnell PA, Dobson RCJ, Perugini MA, Gerrard JA, Hutton CA (2008) Irreversible inhibition of dihydrodipicolinate synthase by 4-oxo-heptenedioic acid analogues. *Bioorg Med Chem* 16:9975–9983
- Bradrick TD, Beechem JM, Howell EE (1996) Unusual binding stoichiometries and cooperativity are observed during binary and ternary complex formation in the single active pore of R67 dihydrofolate reductase, a D2 symmetric protein. *Biochemistry* 35:11414–11424
- Brinch-Pedersen H, Galili G, Knudsen S, Holm PB (1996) Engineering of the aspartate family biosynthetic pathway in barley (*Hordeum vulgare* L.) by transformation with heterologous genes encoding feed-back-insensitive aspartate kinase and dihydrodipicolinate synthase. *Plant Mol Biol* 32:611–620
- Burgess BR, Dobson RC, Bailey MF, Atkinson SC, Griffin MD, Jameson GB, Parker MW, Gerrard JA, Perugini MA (2008)

- Structure and evolution of a novel dimeric enzyme from a clinically important bacterial pathogen. *J Biol Chem* 283:27598–27603
- Cahyanto MN, Kawasaki H, Nagashio M, Fujiyama K, Seki T (2006) Regulation of aspartokinase, aspartate semialdehyde dehydrogenase, dihydrodipicolinate synthase and dihydrodipicolinate reductase in *Lactobacillus plantarum*. *Microbiology* 152:105–112
- Chen VB, Arendall WB 3rd, Headd JJ, Keedy DA, Immormino RM, Kapral GJ, Murray LW, Richardson JS, Richardson DC (2010) MolProbity: all-atom structure validation for macromolecular crystallography. *Acta Crysta D* 66:12–21
- Collaborative Computational Project Number 4 (1994) The CCP4 suite: programs for protein crystallography. *Acta Crysta D* 50:760–763
- Cornish-Bowden A (1976) Principles of enzyme kinetics. Butterworths, London
- Cox RJ, Sutherland A, Vederas JC (2000) Bacterial diaminopimelate metabolism as a target for antibiotic design. *Bioorg Med Chem* 8:843–871
- Cremier J, Treptow C, Eggeling L, Sahm H (1988) Regulation of enzymes of lysine biosynthesis in *Corynebacterium glutamicum*. *J Gen Microbiol* 134:3221–3229
- Davis AJ, Perugini MA, Smith BJ, Stewart JD, Ilg T, Hodder AN, Handman E (2004) Properties of GDP-mannose pyrophosphorylase, a critical enzyme and drug target in *Leishmania mexicana*. *J Biol Chem* 279:12462–12468
- Demeler B (2005a) Bioinformatics basics: applications in biological science and medicine. In: Rashidi H, Buehler L (eds) Hydrodynamic methods. CRC Press LLC, New York, pp 226–255
- Demeler B (2005b) Ultrascan: a comprehensive data analysis software package for analytical ultracentrifugation experiments. Royal Society of Chemistry, Cambridge
- Demeler B, van Holde KE (2004) Sedimentation velocity analysis of highly heterogeneous systems. *Anal Biochem* 335:279–288
- Dereppe C, Bold G, Ghisalba O, Ebert E, Schar HP (1992) Purification and characterization of dihydrodipicolinate synthase from pea. *Plant Physiol* 98:813–821
- Devenish SR, Gerrard JA, Jameson GB, Dobson RC (2008) The high-resolution structure of dihydrodipicolinate synthase from *Escherichia coli* bound to its first substrate, pyruvate. *Acta Crystallogr Sect F Struct Biol Cryst Commun* 64:1092–1095
- Devenish SR, Huisman FH, Parker EJ, Hadfield AT, Gerrard JA (2009) Cloning and characterization of dihydrodipicolinate synthase from the pathogen *Neisseria meningitidis*. *Biochim Biophys Acta* 1794:1168–1174
- Dobson RC, Valegard K, Gerrard JA (2004) The crystal structure of three site-directed mutants of *Escherichia coli* dihydrodipicolinate synthase: further evidence for a catalytic triad. *J Mol Biol* 338:329–339
- Dobson RC, Devenish SR, Turner LA, Clifford VR, Pearce FG, Jameson GB, Gerrard JA (2005a) Role of arginine 138 in the catalysis and regulation of *Escherichia coli* dihydrodipicolinate synthase. *Biochemistry* 44:13007–13013
- Dobson RC, Griffin MD, Jameson GB, Gerrard JA (2005b) The crystal structures of native and (S)-lysine-bound dihydrodipicolinate synthase from *Escherichia coli* with improved resolution show new features of biological significance. *Acta Crysta D* 61:1116–1124
- Dobson RC, Griffin MD, Devenish SR, Pearce FG, Hutton CA, Gerrard JA, Jameson GB, Perugini MA (2008) Conserved main-chain peptide distortions: a proposed role for Ile203 in catalysis by dihydrodipicolinate synthase. *Protein Sci* 17:2080–2090
- Dogovski C, Atkinson SC, Dommaraju SR, Hor L, Hutton CA, Gerrard JA, Perugini MA (2009) Lysine biosynthesis in bacteria—an uncharted pathway for novel antibiotic design in biotechnology: fundamentals and modern development part I. In: Doelle H (ed) Encyclopedia of life support systems (EOLSS). Eolss Publishers, Oxford, pp 116–136
- Dogovski C, Atkinson SC, Dommaraju SR, Downton M, Hor L, Moore S, Paxman JJ, Pevereli MG, Qiu TW, Reumann M, Siddiqui T, Taylor NL, Wagner J, Wubben JM, Perugini MA (2012) Enzymology of bacterial lysine biosynthesis. In: Ekinici D (ed) Biochemistry. InTech Open Access Publisher, Rijeka, pp 225–262
- Domigan LJ, Scally SW, Fogg MJ, Hutton CA, Perugini MA, Dobson RC, Muscroft-Taylor AC, Gerrard JA, Devenish SR (2009) Characterisation of dihydrodipicolinate synthase (DHDPS) from *Bacillus anthracis*. *Biochim Biophys Acta* 1794:1510–1516
- Emsley P, Cowtan K (2004) Coot: model-building tools for molecular graphics. *Acta Crystallogr D* 60:2126–2132
- Evans P (2006) Scaling and assessment of data quality. *Acta Crysta D* 62:72–82
- Evans G, Pettifer RF (2001) CHOOCH: a program for deriving anomalous-scattering factors from X-ray fluorescence spectra. *J Appl Crystallogr* 34:82–86
- Frankard V, Ghislain M, Jacobs M (1992) Two feedback-insensitive enzymes of the aspartate pathway in *Nicotiana sylvestris*. *Plant Physiol* 99:1285–1293
- Frisch DA, Gengenbach BG, Tommey AM, Sellner JM, Somers DA, Myers DE (1991) Isolation and characterization of dihydrodipicolinate synthase from maize. *Plant Physiol* 96:444–452
- Galili G (1995) Regulation of lysine and threonine synthesis. *Plant Cell* 7:899–906
- Ghislain M, Frankard V, Jacobs M (1990) Dihydrodipicolinate synthase of *Nicotiana sylvestris*, a chloroplast-localized enzyme of the lysine pathway. *Planta* 180:480–486
- Ghislain M, Frankard V, Jacobs M (1995) A dinucleotide mutation in dihydrodipicolinate synthase of *Nicotiana sylvestris* leads to lysine overproduction. *Plant J* 8:733–743
- Girish TS, Sharma E, Gopal B (2008) Structural and functional characterization of *Staphylococcus aureus* dihydrodipicolinate synthase. *FEBS Lett* 582:2923–2930
- Griffin MD, Dobson RC, Pearce FG, Antonio L, Whitten AE, Liew CK, Mackay JP, Trehwella J, Jameson GB, Perugini MA, Gerrard JA (2008) Evolution of quaternary structure in a homotetrameric enzyme. *J Mol Biol* 380:691–703
- Griffin MD, Dobson RC, Gerrard JA, Perugini MA (2010) Exploring the dihydrodipicolinate synthase tetramer: how resilient is the dimer–dimer interface? *Arch Biochem Biophys* 494:58–63
- Griffin MDW, Billakanti JM, Wason A, Keller S, Mertens HDT, Atkinson SC, Dobson RCJ, Perugini MA, Gerrard JA, Pearce FG (2012) Characterisation of the first enzymes committed to lysine biosynthesis in *Arabidopsis thaliana*. *PLoS One* 7:e40318
- Halling SM, Stahly DP (1976) Dihydrodipicolinic acid synthase of *Bacillus licheniformis*. Quaternary structure, kinetics, and stability in the presence of sodium chloride and substrates. *Biochim Biophys Acta* 452:580–596
- Hill AV (1910) The possible effects of the aggregation of the molecules of haemoglobin on its dissociation curves. *J Physiol* 40(Suppl):iv–vii
- Hoganson DA, Stahly DP (1975) Regulation of dihydrodipicolinate synthase during growth and sporulation of *Bacillus cereus*. *J Bacteriol* 124:1344–1350
- Humphrey W, Dalke A, Schulten K (1996) VMD: visual molecular dynamics. *J Mol Graph* 14:33–38
- Hutton CA, Perugini MA, Gerrard JA (2007) Inhibition of lysine biosynthesis: an evolving antibiotic strategy. *Mol Biosyst* 3:458–465
- Igartuburu JM, del Río RM, Massanet GM, Montiel JA, Pando E, Luis FR (1991) Study of agricultural by-products. Extractability and amino acid composition of grapeseed (*Vitis vinifera*) proteins. *J Sci Food Agric* 54:489–493

- Kefala G, Evans GL, Griffin MD, Devenish SR, Pearce FG, Perugini MA, Gerrard JA, Weiss MS, Dobson RC (2008) Crystal structure and kinetic study of dihydrodipicolinate synthase from *Mycobacterium tuberculosis*. *Biochem J* 411:351–360
- Krissinel E, Henrick K (2007) Inference of macromolecular assemblies from crystalline state. *J Mol Biol* 372:774–797
- Kumpaisal R, Hashimoto T, Yamada Y (1987) Purification and characterization of dihydrodipicolinate synthase from wheat suspension cultures. *Plant Physiol* 85:145–151
- Kwon T, Sasahara T, Abe T (1995) Lysine accumulation in transgenic tobacco expressing dihydrodipicolinate synthase of *Escherichia coli*. *J Plant Physiol* 146:615–621
- Laue TM, Shah BD, Ridgeway TM, Pelletier SL (1992) Analytical ultracentrifugation in biochemistry and polymer science. The Royal Society of Chemistry, Cambridge, pp 90–125
- Leslie AGW, Powell HR (2007) Processing diffraction data with mosflm. In: Read RJ, Sussman JL (eds) *Evolving methods for macromolecular crystallography*. Springer, Dordrecht, pp 41–51
- MacKerell AD, Bashford D, Bellott M, Dunbrack RL, Evanseck JD, Field MJ, Fischer S, Gao J, Guo H, Ha S, Joseph-McCarthy D, Kuchnir L, Kuczera K, Lau FTK, Mattos C, Michnick S, Ngo T, Nguyen DT, Prodhom B, Reiher WE, Roux B, Schlenkrich M, Smith JC, Stote R, Straub J, Watanabe M, Wiórkiewicz-Kuczera J, Yin D, Karplus M (1998) All-atom empirical potential for molecular modeling and dynamics studies of proteins. *J Phys Chem* 102:3586–3616
- Matthews BF, Widholm JM (1979) Expression of aspartokinase, dihydrodipicolinic acid synthase and homoserine dehydrogenase during growth of carrot cell suspension cultures on lysine- and threonine-supplemented media. *Z Naturforsch C* 34:1177–1185
- McCoy AJ, Grosse-Kunstleve RW, Adams PD, Winn MD, Storoni LJ, Read RJ (2007) Phaser crystallographic software. *J Appl Crystallogr* 40:658–674
- McPhillips TM, McPhillips SE, Chiu HJ, Cohen AE, Deacon AM, Ellis PJ, Garman E, Gonzalez A, Sauter NK, Phizackerley RP, Soltis SM, Kuhn P (2002) Blu-Ice and the distributed control system: software for data acquisition and instrument control at macromolecular crystallography beamlines. *J Synchrotron Radiat* 9:401–406
- Mirwaldt C, Korndorfer I, Huber R (1995) The crystal structure of dihydrodipicolinate synthase from *Escherichia coli* at 2.5 Å resolution. *J Mol Biol* 246:227–239
- Mitsakos V, Dobson RCJ, Pearce FG, Devenish SR, Evans GL, Burgess BR, Perugini MA, Gerrard JA, Hutton CA (2008) Inhibiting dihydrodipicolinate synthase across species: towards specificity for pathogens? *Bioorg Med Chem Lett* 18:842–844
- Murshudov GN, Vagin AA, Dodson EJ (1997) Refinement of macromolecular structures by the maximum-likelihood method. *Acta Crysta D* 53:240–255
- Muscroft-Taylor AC, Soares da Costa TP, Gerrard JA (2010) New insights into the mechanism of dihydrodipicolinate synthase using isothermal titration calorimetry. *Biochimie* 92:254–262
- Negrutiu I, Cattoir-Reynearts A, Verbruggen I, Jacobs M (1984) Lysine overproducer mutants with an altered dihydrodipicolinate synthase from protoplast culture of *Nicotiana glauca*. *Theor Appl Genet* 68:11–20
- Nicholson K, Tarlyn N, Armour T, Swanson M, Dhingra A (2012) Effect of phyllotactic position and cultural treatments toward successful direct shoot organogenesis in dwarf ‘Pixie’ grapevine (*Vitis vinifera* L.). *Plant Cell Tissue Organ Cult (PCTOC)* 111:123–129
- Nunan KJ, Sims IM, Bacic A, Robinson SP, Fincher GB (1997) Isolation and characterization of cell walls from the mesocarp of mature grape berries (*Vitis vinifera*). *Planta* 203:93–100
- Perl A, Shaul O, Galili G (1992) Regulation of lysine synthesis in transgenic potato plants expressing a bacterial dihydrodipicolinate synthase in their chloroplasts. *Plant Mol Biol* 19:815–823
- Perugini MA, Schuck P, Howlett GJ (2000) Self-association of human apolipoprotein E3 and E4 in the presence and absence of phospholipid. *J Biol Chem* 275:36758–36765
- Perugini MA, Griffin MDW, Smith BJ, Webb LE, Davis AJ, Handman E, Gerrard JA (2005) Insight into the self-association of key enzymes from pathogenic species. *Eur Biophys J* 34:469–476
- Phenix CP, Palmer DR (2008) Isothermal titration microcalorimetry reveals the cooperative and noncompetitive nature of inhibition of *Sinorhizobium meliloti* L5–30 dihydrodipicolinate synthase by (S)-lysine. *Biochemistry* 47:7779–7781
- Phillips JC, Braun R, Wang W, Gumbart J, Tajkhorshid E, Villa E, Chipot C, Skeel RD, Kale L, Schulten K (2005) Scalable molecular dynamics with NAMD. *J Comp Chem* 26:1781–1802
- Ricard J, Cornish-Bowden A (1987) Co-operative and allosteric enzymes: 20 years on. *Eur J Biochem* 166:255–272
- Sarrobet C, Thibaud MC, Contard-David P, Gineste S, Bechtold N, Robaglia C, Nussaume L (2000) Identification of an *Arabidopsis thaliana* mutant accumulating threonine resulting from mutation in a new dihydrodipicolinate synthase gene. *Plant J* 24:357–367
- Shaul O, Galili G (1992a) Increased lysine synthesis in tobacco plants that express high levels of bacterial dihydrodipicolinate synthase in their chloroplasts. *Plant J* 2:203–209
- Shaul O, Galili G (1992b) Threonine overproduction in transgenic tobacco plants expressing a mutant desensitized aspartate kinase of *Escherichia coli*. *Plant Physiol* 100:1157–1163
- Shaul O, Galili G (1993) Concerted regulation of lysine and threonine synthesis in tobacco plants expressing bacterial feedback-insensitive aspartate kinase and dihydrodipicolinate synthase. *Plant Mol Biol* 23:759–768
- Shaver JM, Bittel DC, Sellner JM, Frisch DA, Somers DA, Gengenbach BG (1996) Single-amino acid substitutions eliminate lysine inhibition of maize dihydrodipicolinate synthase. *Proc Natl Acad Sci USA* 93:1962–1966
- Silk GW, Matthews BF (1997) Soybean *dapA* mutations encoding lysine-insensitive dihydrodipicolinate synthase. *Plant Mol Biol* 33:931–933
- Soares da Costa TP, Muscroft-Taylor AC, Dobson RCJ, Devenish SRA, Jameson GB, Gerrard JA (2010) How essential is the ‘essential’ active-site lysine in dihydrodipicolinate synthase? *Biochimie* 92:837–845
- Sreerama N, Woody RW (2000) Estimation of protein secondary structure from circular dichroism spectra: comparison of CONTIN, SELCON, and CDSSTR methods with an expanded reference set. *Anal Biochem* 287:252–260
- Turnbull WB, Daranas AH (2003) On the value of c: can low affinity systems be studied by isothermal titration calorimetry? *J Am Chem Soc* 125:14859–14866
- van der Meer IM, Bovy AG, Bosch D (2001) Plant-based raw material: improved food quality for better nutrition via plant genomics. *Curr Opin Biotechnol* 12:488–492
- Vauterin M, Jacobs M (1994) Isolation of a poplar and an *Arabidopsis thaliana* dihydrodipicolinate synthase cDNA clone. *Plant Mol Biol* 25:545–550
- Vauterin M, Frankard V, Jacobs M (2000) Functional rescue of a bacterial *dapA* auxotroph with a plant cDNA library selects for mutant clones encoding a feedback-insensitive dihydrodipicolinate synthase. *Plant J* 21:239–248
- Vivier MA, Pretorius IS (2002) Genetically tailored grapevines for the wine industry. *Trends Biotechnol* 20:472–478
- Voss JE, Scally SW, Taylor NL, Atkinson SC, Griffin MD, Hutton CA, Parker MW, Alderton MR, Gerrard JA, Dobson RC, Dogovski C, Perugini MA (2010) Substrate-mediated



- stabilization of a tetrameric drug target reveals Achilles heel in anthrax. *J Biol Chem* 285:5188–5195
- Wallsgrave RM, Mazelis M (1980) The enzymology of lysine biosynthesis in higher plants: complete localization of the regulatory enzyme dihydrodipicolinate synthase in the chloroplasts of spinach leaves. *FEBS Lett* 116:189–192
- Webster FH, Lechowich RV (1970) Partial purification and characterization of dihydrodipicolinic acid synthetase from sporulating *Bacillus megaterium*. *J Bacteriol* 101:118–126
- Yamakura F, Ikeda Y, Kimura K, Sasakawa T (1974) Partial purification and some properties of pyruvate-aspartic semialdehyde condensing enzyme from sporulating *Bacillus subtilis*. *J Biochem* 76:611–621
- Yugari Y, Gilvarg C (1965) The condensation step in diaminopimelate synthesis. *J Biol Chem* 240:4710–4716
- Zhu X, Galili G (2003) Increased lysine synthesis coupled with a knockout of its catabolism synergistically boosts lysine content and also transregulates the metabolism of other amino acids in *Arabidopsis* seeds. *Plant Cell* 15:845–853